A Robust 5 MW Split-Pole Reluctance Synchronous Wind Generator

Jandré Dippenaar, *Student Member, IEEE* and Maarten J. Kamper, *Senior Member, IEEE*

***Abstract*—In this paper the consequences for the performance of a reluctance synchronous wind generator, when removing some complexity from its rotor, are considered. The investigation is done on a 5 MW power level with the generator in the medium speed range. Complex flux barrier shapes are avoided in the designs. As a result, a reluctance generator with a simple salient pole rotor is optimized in its design and used as a baseline machine. Skewing and a fractional slot winding is implemented to address a high torque ripple. Finally, a suggested split-pole design is shown to increase the efficiency of the simple reluctance generator to above 98% with a torque ripple below 5% and a power factor of around 0.65.**

***Index Terms*—Wind energy, wind generators, reluctance synchronous, split-pole, design optimization.**

I. Introduction

THE world is in search of more sustainable and environmentally friendly solutions to meet the need of a growing energy demand. One of these proposed solutions is wind energy. Wind energy has recently experienced remarkable growth, with offshore technologies alone growing 30% per year from 2010 to 2018 [1]. The size of both on- and offshore turbines are increasing, with *offshore* turbines breaking the 10 MW mark and manufacturers such as *GE*, *Vestas* and *Siemens Gamesa* all offering *onshore* turbines reaching 5 MW.

Furthermore, there is a growth in the use of full-rated power converters as an interface between the generator and the power grid in renewable energy systems such as wind- and hydro-energy generation [2], [3]. With the use of these power converters maximum torque per ampere and adjustable speed can be achieved. The generators can be connected to the turbines either directly or via gearboxes. The direct-drive solution can be associated with an increase in generator mass, while a high-speed gearbox can decrease reliability. As a result, the medium-speed gearbox has drawn some attention for wind generation systems, as a well-balanced trade-off between mass and reliability [4], [2]. As an example, the *Vestas V164-9.5* MW turbine has a rated speed of 400 r/min, a maximum speed of 536 r/min and uses a 3 stage planetary differential gearbox with a 1:38.03 gear ratio [5]. The medium-speed range for wind generators is, in general, taken as between 100- and 500 r/min.

Another trend involves the search for non-permanent magnet generator solutions, even though permanent magnet generators offer good power density and efficiency. Magnets are typically expensive, and even the more affordable ferrite magnets run the risk of demagnetization, making a non-permanent magnet solution more robust. Non-permanent magnet generators include, inter alia, induction generators, wound-rotor synchronous generators and switched reluctance generators. The use of reluctance synchronous generators (RSGs) for wind energy generation has attracted attention at a 5 MW power level [6], [7]. The conductor-less iron rotor, good efficiency and standard converter make the RSG very attractive to use. Considering the trends mentioned, the focus of this paper is therefore on the RSG designed for a medium-speed wind generator at 5 MW.

High torque ripple is a well known problem of RSGs. A fractional slot winding has proven to decrease torque ripple in Reluctance Synchronous Machines (RSMs) [8]. Rotor skewing has been proven to have the same effect. While some researchers cite a single slot pitch skew angle as conventional, others have found that the optimum skew angle can be machine specific. In this paper the optimum skew angle for the salient pole type RSG is briefly investigated and implemented in simulation and design optimization.

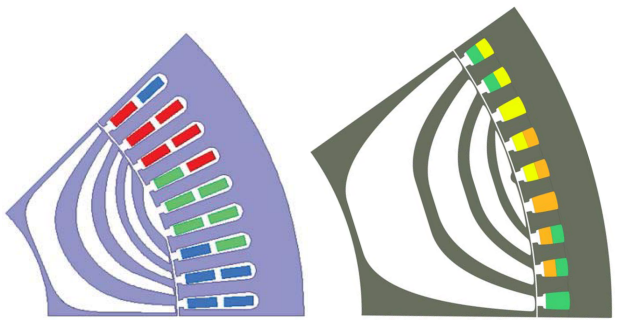

(a) (b)

Fig. 1. Cross-sections of 5 MW designs of (a) the 8-pole generator of [6] and (b) the 10-pole generator of [7].

The authors acknowledge the financial contribution of the Centre for Renewable and Sustainable Energy Studies (CRSES) at Stellenbosch University in South Africa.

Jandré Dippenaar and Maarten J. Kamper are with the Department of Electrical and Electronic Engineering, Stellenbosch University, Stellenbosch, South Africa, phone: +27(0)21-808-4323; fax: +27(0)21-808-3951; e-mail: jandredippenaar@gmail.com, kamper@sun.ac.za.

978-1-7281-9944-3/20/$31.00 ©2020 IEEE

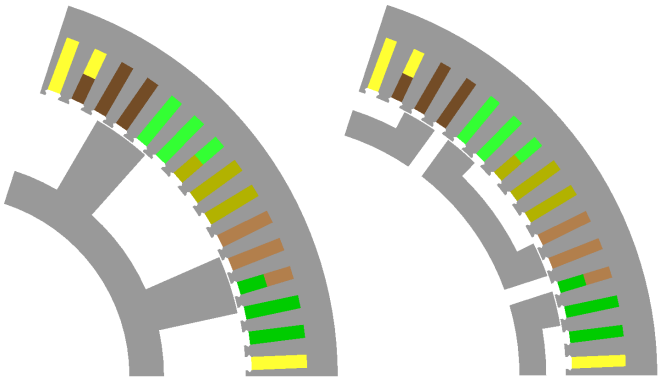

(a) (b)

Fig. 2. Optimized RSG segments of (a) the salient pole RSG and (b) the split-pole RSG.

Both [6] and [7] uses rotor flux barriers, as shown in Fig. 1, which are commonly found in RSGs. Flux barriers weaken the structural integrity of the rotor and proper machine operation requires a level of structural integrity to be maintained. Therefore assuming mechanical feasibility or no deformation under peak load, as in [7], can be detrimental. The thin ribs of the flux barriers are especially susceptible to deformation under loading as seen in [9]. In this paper, a step is taken away from typical flux barriers by incorporating a salient pole rotor RSG, as shown in Fig. 2a, that offers ease of manufacture and is robust in operation.

Flux barriers can be present in various quantities and have different geometries ranging from incredibly complex, as in [10], to fairly simple, as in [11]. In this paper, the flux-barrier concept is additionally utilized by splitting the rotor poles, in order to limit the q-axis flux linkage and increase the d-axis flux linkage, as in [12] and shown in Fig. 2b. Finally, suggestions are made regarding the manufacturing of the presented split-pole machine.

II. Modelling the RSG

The modelling of the RSG is based on the dq0 equivalent circuits in Fig. 3. The dq0 transformation is used to represent the machine equations in the synchronously-rotating reference frame with respect to the rotor. We will assume a balanced system and therefore the 0-component, resulting from the dq0 transformation, is absent.

The equations are derived as if the machine is operating in motor mode. To operate as a generator, negative q-axis current is supplied, as Fig. 4 illustrates. Fig. 4 also shows the power factor angle, as represented by ϕ, and the current angle, under converter control, as represented by θ. The RSG has no rotor field-component and the equations for the d- and q-axis supply voltages under steady state conditions are,

$$V_d = R_s I_{d1} - \omega_e \lambda_q - L_e I_{q1} \omega_e, \tag{1}$$

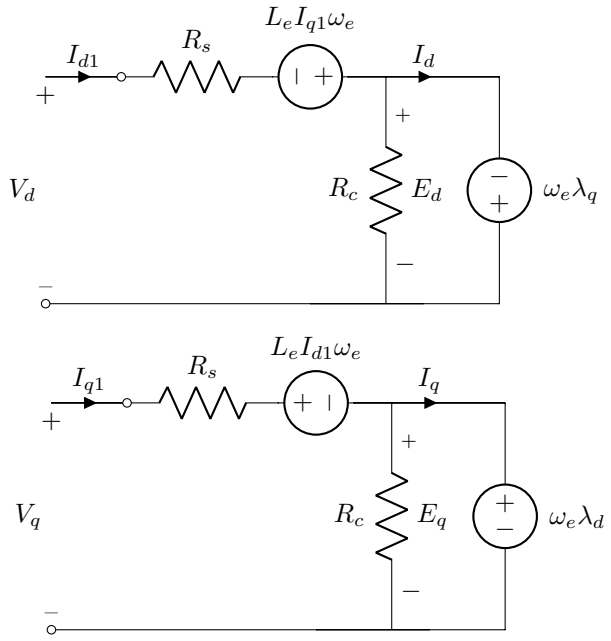

Fig. 3. Equivalent DQ circuits of the RSG.

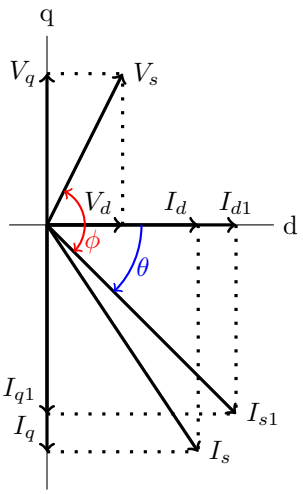

Fig. 4. Space phasor diagram of the RSG.

$$V_q = R_s I_{q1} + \omega_e \lambda_d + L_e I_{d1} \omega_e. \tag{2}$$

In (1) and (2), ω_e is the electrical angular velocity, R_s is the stator winding resistance and L_e is the end-winding leakage inductance, which is calculated with the method of [13]. The d- and q-axis flux linkages values, given by λ_d and λ_q, includes both the main flux and the leakage flux of the generator.

The d- and q-axis inductances are determined by

$$L_d = \frac{\lambda_d}{I_d}, \tag{3}$$

$$L_q = \frac{\lambda_q}{I_q}. \tag{4}$$

The contribution of the core losses are taken into account by R_c in the equivalent circuits of Fig. 3 and is determined by,

$$R_c = \frac{3E_a^2}{P_{core}}, \tag{5}$$

where E_a is the RMS value of the speed voltages (E_d, E_q) and given by

$$E_a = \sqrt{\frac{1}{2}(E_d^2 + E_q^2)}. \tag{6}$$

The torque acting to decelerate the rotor of the RSG is given by

$$T_e = \frac{3}{4}p(\lambda_d I_q - \lambda_q I_d). \tag{7}$$

A modified version of Steinmetz's core loss equation is used to determine the core losses:

$$P_{core} = c f_1^x (B_{tooth}^y M_{tooth} + B_{yoke}^y M_{yoke}) k_{exp}. \tag{8}$$

The Steinmetz coefficients are c, x and y and can be found by measurements and loss frequency curves at the fundamental supply frequency, f_1. The parameters B_{tooth} and B_{yoke} are the maximum flux densities in the tooth and yoke respectively, obtained from the FEM software. M_{tooth} and M_{yoke} are the masses of the teeth and the yoke respectively.

The resistance of the copper windings in the stator is calculated clasically by

$$R_s = \frac{2W\rho_t(l + l_e)}{n_a \frac{A_{cu}}{z}}. \tag{9}$$

III. RSG Simulation

The RSGs of Fig. 2 are simulated with an in-house finite element (FEM) package. A brief mesh independence study was done in order to decrease simulation time and still maintain accuracy. The generator volume and pole number is based on the 5 MW RSG of [7], further elaborated in [14], in order to compare the two machines. Reference [6] also presents a 5 MW RSG, but the given torque density of 52 kNm/mm^3 is questionable. This is quite high for a RSG, but could potentially be explained by the requirement of water cooling.

Feasible peak current densities of $J = 2\ A/mm^2$ and electrical loading less than $A = 80\ kA/m$, to have feasible AJ values, are used in the proposed salient pole ans split-pole RSG designs to enable air cooling. A stator slot fill factor of 0.6 was found to be consistent with [15] for large machines with straight, open stator slots. It is slightly more conservative than the 0.65 fill factor used in [16]. A slightly more conservative airgap of 3 mm is used, in line with [6].

The RSG is optimized using the multi-objective, non-dominant sorting genetic algorithm (NSGA-II) of a commercial optimization package called *VisualDoc*. In the *VisualDoc* software, optimization objectives and constraints are specified. *VisualDoc* manages the optimization procedure and is connected to a Python script, which in turn connects with the FEM package. The optimization consists only of a single objective; maximizing the power factor:

$$F(X) = maximize\left[PF\right]. \tag{10}$$

This is subject to the following constraints:

$$G(X) = \begin{bmatrix} E_{ff} \geq 98\% \\ P_{out} \approx 5\ \text{MW} \\ T_{ripple} \leq 5\% \end{bmatrix}. \tag{11}$$

Between six and seven physical dimensions, encapsulating the rotor and stator, are used as design variables. An additional design variable is allocated for the current angle, θ.

A known problem with RSMs is a high torque ripple. The torque ripple percentage is calculated by,

$$TR = \frac{T_{max} - T_{min}}{T_{avg}} \times 100, \tag{12}$$

where T_{max}, T_{min} and T_{avg} are the respective maximum, minimum and average torque values obtained from multiple FEM simulation rotor-steps, covering 60 electrical degrees of rotation.

The design optimization of an *unskewed* RSG could not meet the 5% torque ripple requirement. However, skewing, combined with a fractional slot winding, is used to successfully decrease the torque ripple to less than 5%, as shown in Table I.

TABLE I
SIMULATION RESULTS OF FIG. 2A SIMULATED AS 1- AND 2 SLOT PITCH (SP) SKEWED AND UNSKEWED SALIENT POLE MACHINES

	Unit	Skewed		Unskewed
		2 SP	1 SP	
Power output	MW	5.00	5.50	5.68
Torque average	p.u.	1.00	1.10	1.13
Torque ripple	%	4.92	8.74	15.51
Power factor		0.539	0.555	0.561
Efficiency	%	97.94	98.14	98.30

A. Rotor Skewing

For the skewing simulation, 5 sub-machines are evaluated at each simulation step, from step 1 to step *n*. Each simulation step corresponds with a rotational position. The machine parameters at a single simulation step are determined by the average of the 5 sub-machines at that position, as shown in Fig. 5. The final machine performance parameters are made up of the average of all the simulation steps, which are in turn made up of the average of the 5 sub-machine steps at a single position, as illustrated in Fig. 6.

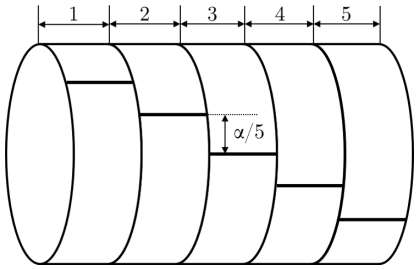

Fig. 5. Skewing with 5 sub-machines, for a single simulation step.

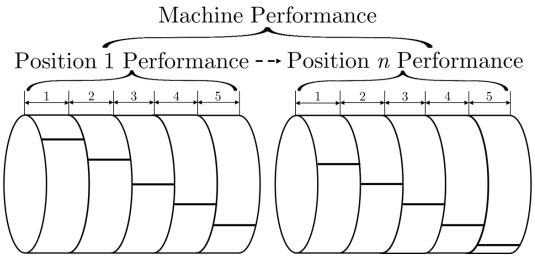

Fig. 6. Machine performance determined from skewing simulation.

If the skew angle is a mechanical angle α, the positional rotation of the 5 sub-machines ($\alpha_{1\to5}$) are given by,

$$\begin{bmatrix}\alpha_1 & \alpha_2 & \alpha_3 & \alpha_4 & \alpha_5\end{bmatrix} = \begin{bmatrix}-2\frac{\alpha}{5} & -\frac{\alpha}{5} & 0 & \frac{\alpha}{5} & 2\frac{\alpha}{5}\end{bmatrix}. \tag{13}$$

The current angle of every sub-machine ($\theta_{1\to5}$) is also modified by adding the corresponding skew angle, converted to electrical degrees (α_e), to the optimum current angle (θ), as follows,

$$\begin{bmatrix}\theta+\alpha_{e1} & \theta+\alpha_{e2} & \theta+\alpha_{e3} & \theta+\alpha_{e4} & \theta+\alpha_{e5}\end{bmatrix}. \tag{14}$$

The 5-sub-machine skew simulation is repeated at a large enough number of different rotational positions, over 60 electrical degrees, to give accurate simulation results. Reference [17] notes that no significant difference in simulation results is found with an increase in the number of sub-machines beyond 5, however, the specific skew angle used does have a significant impact on machine performance.

TABLE II
DESIGN OPTIMIZATION RESULTS OF THE INDIVIDUALLY OPTIMIZED, 1- AND 2 SLOT PITCH (SP) SKEWED, SPLIT-POLE RSGS OF FIG. 2B

	Unit	2 SP Skewed	1 SP Skewed
Pout	MW	5.030	5.007
Torque average	p.u.	97.87	97.32
Torque ripple	%	4.82	5.02
Power factor		0.649	0.648
Efficiency	%	98.15	98.27

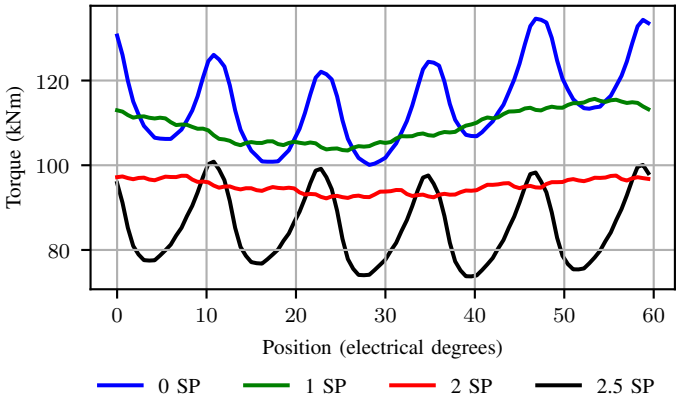

Fig. 7. Instantaneous torque versus rotor position of the split-pole RSG of Fig. 2b with skew angles in terms of slot pitches (SP) as a parameter.

B. *Optimal Skew Angle*

In [18] and [19] it is shown that the torque ripple of RSMs generally decrease with an increase in skew angle. It is also adversely shown that an increase in skew angle corresponds to a decrease in the average torque. This is evident from Table I, for the salient pole RSG of Fig. 2a, and from Fig. 7, for the split-pole RSG of Fig. 2b.

It has been established that the RSGs in Fig. 2 require skewing to decrease the torque ripple to below 5%. The question is then, what is the best skew angle for optimum machine performance? To answer this question, the split-pole RSG in Fig. 2b is optimized at a skew angle of 1 slot pitch and 2 slot pitches respectively.

It is interesting to note that both these skew angles result in two physically different machines, shown in Fig. 8, with similar performance parameters, as seen in Table II. The 2 slot pitch skewed RSG fares slightly better. Although a skew angle of 1 slot pitch is framed as conventional by [20] and [17], the

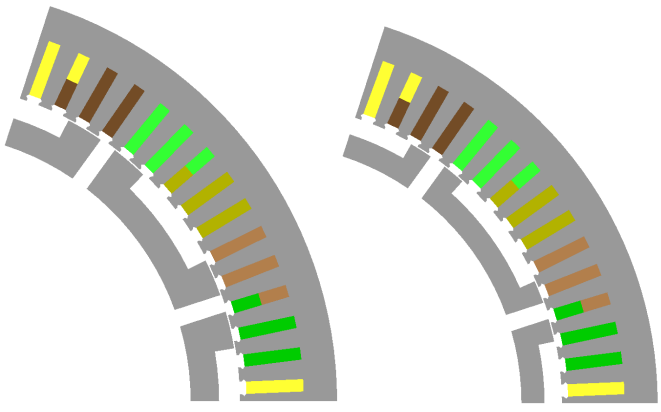

Fig. 8. Optimized split-pole RSG segments of (a) the 2 slot pitch skewed RSG and (b) the 1 slot pitch skewed RSG.

TABLE III
COMPARISON OF RSGS IN FIG. 1B, FIG. 2A AND FIG. 2B

	Unit	RSG of [7]	Salient Pole	Split-Pole
Power out	[MW]	5.05	5.00	5.03
Torque average	[kNm]	98.4	97.57	97.87
Efficiency	[%]	98.0	97.94	98.15
Power factor		0.853	0.539	0.649
Torque Ripple	[%]	-	4.92	4.82
Poles		10	10	10
Slots per pole		9	7.5	7.5
Fill Factor		0.35	0.6	0.6
Stator diameter	[m]	1.89	1.89	1.89
Stack length	[m]	1.88	1.88	1.88
Airgap	[mm]	2.5	3	3
Torque density	[kNm/m^3]	18.65	18.50	18.56
Current angle	[°]	73.4	54.620	63.426
Current density	A/mm^2	4.5	1.414	1.414
Speed	[r/min]	500	500.00	500.00
L_d	[mH]	-	148.05	222.85
L_q	[mH]	-	39.62	44.07
L_d/L_q		-	3.74	5.06
Active Mass	[t]	14.8	21.97	19.42

optimization results concur with [19] and [10] in that 1 slot pitch is not necessarily the optimal skew angle. In a design optimization where skewing is implemented to decrease the torque ripple, it would be prudent to investigate which skewing angle is best for a specific design, with a specific torque ripple requirement.

Furthermore, it was found that care should be taken when selecting a skew angle, as rapid fluctuations in torque can go undetected if too few simulation steps are used. Too few steps would give a seemingly lower, but inaccurate, torque ripple result.

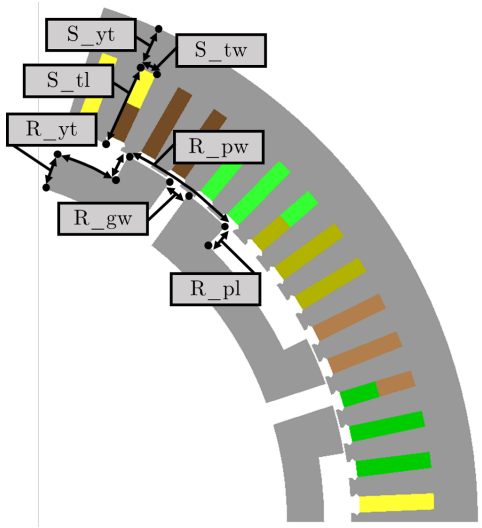

Fig. 9. Cross-section segment of the optimized split-pole RSG illustrating design variables.

TABLE IV
OPTIMIZATION DIMENSIONS OF THE SALIENT POLE AND SPLIT-POLE RSGS

Dimension	Description	Salient Pole [mm]	Split-Pole [mm]
S_yt	Stator yoke thickness	74.1	75.99
S_tw	Stator tooth width	16.07	14.07
S_tl	Stator tooth length	149.46	145.11
R_yt	Rotor yoke thickness	83.8	64.71
R_pw	Rotor pole width	143.32	210.75
R_pl	Rotor pole length	194.7	44.19
R_gw	Rotor gap width	-	39.45
R_ir	Rotor inner radius	439.9	612
R_or	Rotor outer radius	718	720.90

By comparing Table I and Table II, it is clear that at a skewing angle of 2 slot pitches, the split-pole RSG of Fig. 2b offer significant performance benefits over the simple salient pole RSG of Fig. 2a. Although skewing the simple salient pole RSG decreases the torque ripple to acceptable levels, it is evident from Table I that the optimized salient pole RSG still has a low power factor. In an effort to increase the power factor, the split-pole RSG of Fig. 2b is suggested.

IV. SPLIT-POLE RSG

To decrease the q-axis flux linkage and increase the d-axis flux linkage, gaps are inserted in the middle of the salient poles of the rotor. The effects of the gap on the flux linkages, and hence inductances, of the split-pole RSG, compared to the salient pole RSG, can be seen in Table III, where the saliency ratio increases by 35%. The split-pole RSG is optimized with the same optimization constraints and objectives as the salient pole RSG, but the number of variables increases from 6 to 7 in order to accommodate the alternative rotor design, as illustrated in Fig. 9. The optimized dimensions of the salient pole- and split-pole RSGs are given in Table IV.

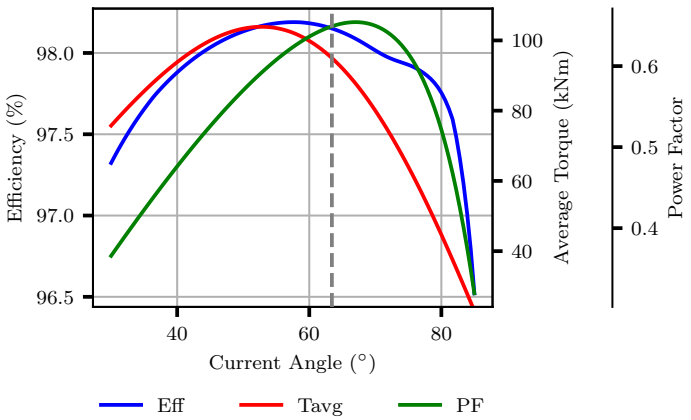

Fig. 10. Performance versus current angle of the optimized split-pole RSG of Fig. 2b.

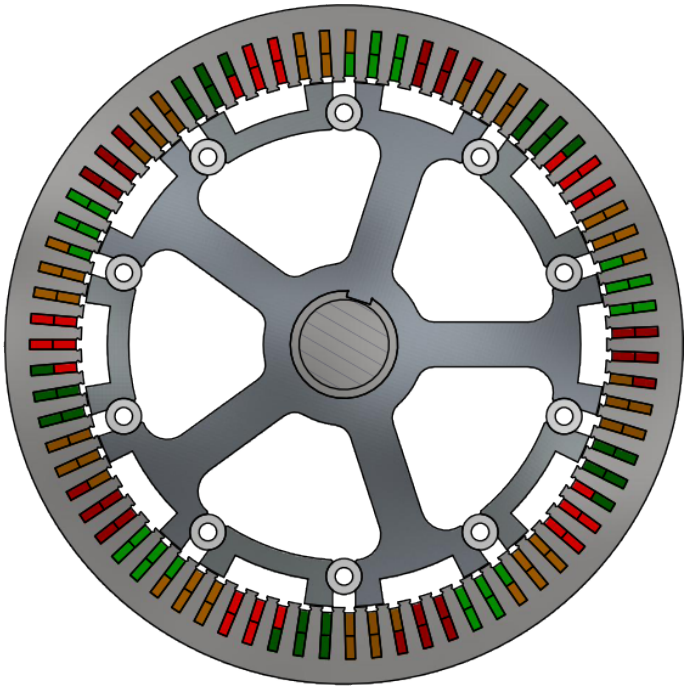

Fig. 11. Mechanically feasible split-pole RSG.

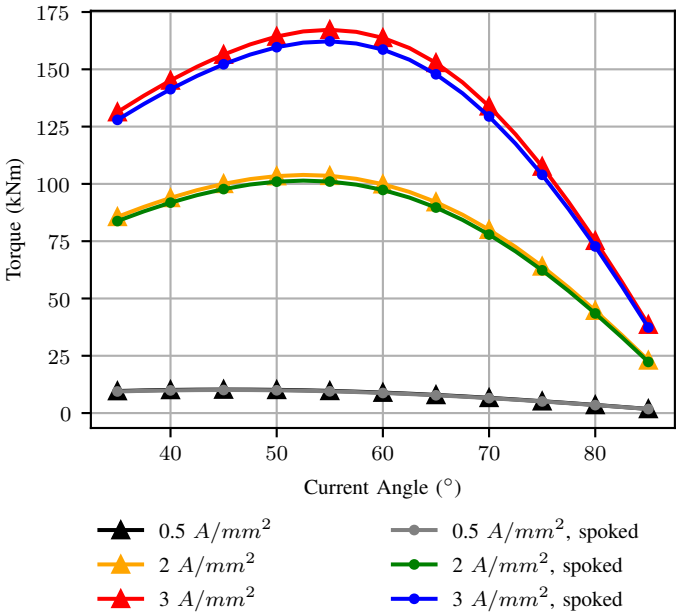

Fig. 13. The effect of different current densities on the average torque versus current angle of the spoked and un-spoked split-pole RSGs.

A. *Performance Results*

The performance of the optimized split-pole RSG can be seen in Fig. 10. It is also compared in Table III with the salient pole RSG and the RSG of [7]. Splitting the poles has the effect of increasing the power factor by about 20%. However, the split-pole design presents a challenge for the physical manufacturing of the rotor.

B. *Manufacturing Suggestions*

For large machines, a spoked arm rotor construction can be considered, as suggested in [16]. Yet, for the split-pole RSG every second pole should not be connected to a spoked arm - if iron is used - otherwise the flux linkage would travel along the spoke and defeat the purpose of the split-pole. A suggested solution can be seen in Fig. 11, where every second pole is keyed to a spoked pole on either side, using a cylindrical key. When assembling a skewed machine, each of the five sub-machine stacks has to be stacked and keyed, before moving on to the next relatively displaced stack.

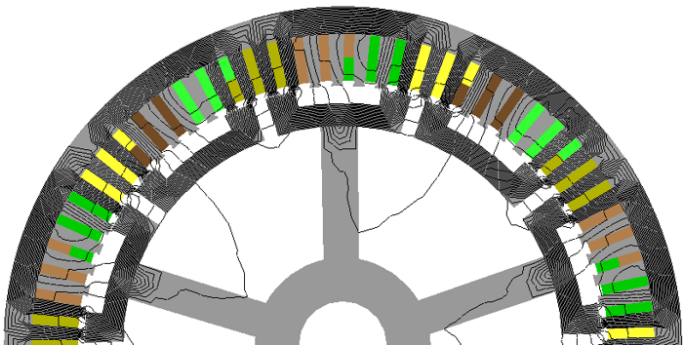

Fig. 12. Flux lines showing the flux leakage for the split-pole RSG.

For a spoked RSG, the effects of the spokes need to be taken into consideration. As can be seen in Fig. 12, the flux lines do not travel along the spokes. However, the simulated results show a decrease in power factor of 3.6% due to increased leakage. As seen in Fig. 13, the effect is larger at higher current densities and higher average torque, which suits the wind generator application as wind turbines operate at partial loading for large portions of time.

Another manufacturing consideration could involve the magnetic isolation of the poles from the spokes, using non-magnetic material. In this case, every pole could have a spoke, instead of having floating poles (poles without spokes) and keys. The flux would then not be able to travel along the spokes, due to the non-magnetic nature of the spokes. To manufacture such a design, spokes would have to be fitted onto both the poles and the shaft. To assemble a skewed machine, the spoked poles can be fixed to the shaft at skewed shaft-spoke connection points. Alternatively, the spokes can be fixed to the shaft linearly, with the spokes being angled towards the top pole-side so that the poles are in the appropriate skewed position.

Another alternative method could involve the use of additive manufacturing as described in [21]. However, it is currently and immature technology and the feasibility of such a design requires further research.

V. Conclusions

Two mechanically-robust and relatively simple rotor structures are considered in this paper in the design of a 5 MW, 10-pole RSG wind generator. These are investigated as alternatives to more complex distributed flux barrier RSGs. The most basic RSG is the salient pole RSG which is then further modified, resulting in a split-pole RSG. From the results, the following conclusions are drawn.

The optimized simple, salient pole design delivers similar torque densities as the distributed flux barrier RSG of [7], with an equivalent volume. However, it yields a low power factor with a larger mass. In an effort to improve the power factor of the salient pole RSG, a split-pole RSG is suggested. This design change improves the L_d/L_q ratio by 35% and improves the power factor by 20%, while maintaining a similar torque density of 18.56 kNm/m^3, efficiency above 98% and torque ripple below 5%.

It is shown that the torque ripple can be decreased to below 5% by using a combination of a stator fractional slot winding and rotor skewing. It is also shown that different skew angles can result in quite different generator designs, while still meeting the design performance requirements. The conventional skew angle of 1 slot pitch does not necessarily yield the best design.

The split-pole RSG presents a potential challenge when it comes to manufacturing, hence suggestions are made in this regard. A spoked-arm rotor with floating poles is suggested as a feasible design. It is shown that the flux lines do not link through the spokes, however, there is an increase in flux leakage and therefore a slight decrease in machine performance. Alternative manufacturing suggestions are made that potentially would not decrease machine performance in this way.

References

[1] IEA, "Offshore Wind outlook 2019," 2019.

[2] V. Yaramasu, B. Wu, P. C. Sen, S. Kouro, and M. Narimani, "High-power wind energy conversion systems: State-of-the-art and emerging technologies," *Proceedings of the IEEE*, vol. 103, pp. 740–788, May 2015.

[3] T. Holzer and A. Muetze, "Full-size converter operation of large hydro power generators: Generator design aspects," in *2018 IEEE Energy Conversion Congress and Exposition (ECCE)*, pp. 7363–7368, Sep. 2018.

[4] S. Wang, A. R. Nejad, and T. Moan, "On design, modelling, and analysis of a 10-mw medium-speed drivetrain for offshore wind turbines," *Wind Energy*.

[5] IECRE, "Wind energy, iecre certificates," 2020.

[6] P. Roshanfekr, S. Lundmark, T. Thiringer, and M. Alatalo, "A synchronous reluctance generator for a wind application-compared with an interior mounted permanent magnet synchronous generator," in *7th IET International Conference on Power Electronics, Machines and Drives (PEMD 2014)*, pp. 1–5, April 2014.

[7] E. Howard and M. J. Kamper, "Reluctance synchronous wind generator design optimisation in the megawatt, medium speed range," in *2017 IEEE Energy Conversion Congress and Exposition (ECCE)*, pp. 1864–1871, Oct 2017.

[8] V. A. Dmitrievskii, V. A. Prakht, and V. M. Kazakbaev, "Ultra premium efficiency (ie5 energy-efficiency class) synchronous reluctance motor with fractional slot winding," in *2018 XIII International Conference on Electrical Machines (ICEM)*, pp. 1015–1020, Sep. 2018.

[9] S. Taghavi and P. Pillay, "A mechanically robust rotor with transverse-laminations for a synchronous reluctance machine for traction applications," in *2014 IEEE Energy Conversion Congress and Exposition (ECCE)*, pp. 5131–5137, Sep. 2014.

[10] E. Howard, M. J. Kamper, and S. Gerber, "Asymmetric flux barrier and skew design optimization of reluctance synchronous machines," *IEEE Transactions on Industry Applications*, vol. 51, pp. 3751–3760, Sep. 2015.

[11] H. Yu, X. Zhang, J. Ji, and L. Xu, "Rotor design to improve torque capability in synchronous reluctance motor," in *2019 22nd International Conference on Electrical Machines and Systems (ICEMS)*, pp. 1–5, Aug 2019.

[12] R. Constancias, I. Rasoanarivo, N. Takorabet, and F. M. Sargos, "Design and optimization of a synchronous reluctance machine with salient poles and flux barriers," in *2010 IEEE Energy Conversion Congress and Exposition*, pp. 2672–2678, Sep. 2010.

[13] M. Kamper, *Design Optimisation of Cageless Flux Barrier Rotor Reluctance Synchronous Machine*. Phd, Stellenbosch University, 1996.

[14] E. Howard, *Design optimisation of Reluctance Synchronous Machines: A Motor and Generator Study*. Phd, Stellenbosch University, 2017.

[15] Ion Boldea and Syed A. Nasar, *The Induction Machine Handbook*. CRC Press, 2002.

[16] L. Sethuraman, M. Maness, and K. L. Dykes, "Optimized generator designs for the dtu 10-mw offshore wind turbine using generatorse: Preprint," in *American Institute of Aeronautics and Astronautics 35th Wind Energy Symposium*, 2017.

[17] X. B. Bomela and M. J. Kamper, "Effect of stator chording and rotor skewing on performance of reluctance synchronous machine," *IEEE Transactions on Industry Applications*, vol. 38, pp. 91–100, Jan 2002.

[18] R. Moghaddam, *Synchronous Reluctance Machine (SynRM) in Variable Speed Drives (VSD) Applications*. Phd, KTH Royal Institute of Technology, 2011.

[19] T. Hubert, M. Reinlein, A. Kremser, and H. . Herzog, "Torque ripple minimization of reluctance synchronous machines by continuous and discrete rotor skewing," in *2015 5th International Electric Drives Production Conference (EDPC)*, pp. 1–7, Sep. 2015.

[20] K. Wang, Z. Zhu, G. Ombach, M. Koch, S. Zhang, and J. Xu, "Torque ripple reduction of synchronous reluctance machines: using asymmetric flux-barrier," *COMPEL*, vol. 34, pp. 18–31, Jan 2015.

[21] R. Wrobel and B. C. Mecrow, "A comprehensive review of additive manufacturing in construction of electrical machines," *IEEE Transactions on Energy Conversion*, pp. 1–1, 2020.

VI. Biographies

Jandré Dippenaar received the B.Eng degree in Mechatronic Engineering from Stellenbosch University, South Africa, in 2017. He is currently working towards the completion of the M.Eng degree at the Department of Electrical and Electronic Engineering at Stellenbosch University. His current research focus is on the design of synchronous reluctance machines in the megawatt range, for applications in renewable energy.

Maarten J. Kamper received the M.Sc. (Eng) and Ph.D. (Eng) degrees from the Stellenbosch University, South Africa, in 1987 and 1996, respectively. In 1989, he joined the academic staff of the Department of Electrical and Electronic Engineering, Stellenbosch University, where he is currently a Professor of electrical machines and drives. His research area is computer aided design and the control of reluctance, permanent magnet, and induction electrical machine drives, with applications in electric transportation and renewable energy. Prof. Kamper is a South African National Research Foundation supported scientist and a registered Professional Engineer in South Africa.